arXiv:1304.2236v1 [cond-mat.mes-hall] 8 Apr 2013

Doping Mechanisms in Graphene-MoS_2 Hybrids

B. Sachs,[*,†] L. Britnell,[‡] T. O. Wehling,[¶] A. Eckmann,[‡] R. Jalil,[‖] B. D. Belle,[‖] A. I. Lichtenstein,[†] M. I. Katsnelson,[⊥] and K. S. Novoselov[‡]

I. Institut für Theoretische Physik, Universität Hamburg, Jungiusstraße 9, D-20355 Hamburg, Germany, School of Physics and Astronomy, University of Manchester, M13 9PL, Manchester, United Kingdom, Institut für Theoretische Physik, Universität Bremen, Otto-Hahn-Allee 1, D-28359 Bremen, Germany, Bremen Center for Computational Materials Science, Universität Bremen, Am Fallturm 1a, D-28359 Bremen, Germany, Manchester Centre for Mesoscience and Nanotechnology, University of Manchester, Manchester M13 9PL, United Kingdom, and Radboud University of Nijmegen, Institute for Molecules and Materials, Heijendaalseweg 135, 6525 AJ Nijmegen, The Netherlands

E-mail: bsachs@physnet.uni-hamburg.de

Abstract

We present a joint theoretical and experimental investigation of charge doping and electronic potential landscapes in hybrid structures composed of graphene and semiconducting single layer MoS_2. Combining density functional theory with Raman and photovoltaic experiments, we show that impurities in MoS_2 induce electron doping of graphene. Furthermore, we

---

[*] To whom correspondence should be addressed

[†] I. Institut für Theoretische Physik, Universität Hamburg, Jungiusstraße 9, D-20355 Hamburg, Germany

[‡] School of Physics and Astronomy, University of Manchester, M13 9PL, Manchester, United Kingdom

[¶] Institut für Theoretische Physik, Universität Bremen, Otto-Hahn-Allee 1, D-28359 Bremen, Germany

[§] Bremen Center for Computational Materials Science, Universität Bremen, Am Fallturm 1a, D-28359 Bremen, Germany

[‖] Manchester Centre for Mesoscience and Nanotechnology, University of Manchester, Manchester M13 9PL, United Kingdom

[⊥] Radboud University of Nijmegen, Institute for Molecules and Materials, Heijendaalseweg 135, 6525 AJ Nijmegen, The Netherlands

find that MoS_2 edges give rise to charge reordering and a potential shift in graphene, which can be controlled through external gate voltages. The interplay of edge and impurity effects allows to use the graphene-MoS_2 hybrid as a photodetector. Spatially resolved photocurrent signals can be used to resolve potential gradients and local doping levels in the sample.

Being a truly two-dimensional material,[1] graphene can be integrated into hybrid structures with other 2D crystals such as boron nitride (BN), tungsten disulfide (WS_2) or molybdenum disulfide (MoS_2).[2–5] The ability to build ’on demand’ complex heterostructures via layer-by-layer integration establishes a whole family of new materials with widely varying characteristics and exciting possibilities for novel 2D nanodevices.[6,7] A prerequisite for future electronic applications lies in the understanding of interface effects when different building blocks come together. In particular, the electronic properties of realistic interfaces of graphene and two-dimensional materials present an open problem.

In this work, we investigate heterostructures made of graphene and the semiconducting transition metal dichalcogenide MoS_2, a system that has already been utilized for vertical field-effect transistors.[3] We study how different charge transfer mechanisms control relative Fermi level positions, built-in electric fields and charge reordering at realistic graphene-MoS2 interfaces. The simulated charge and potential landscapes are compared to Raman and photovoltaic measurements.

In order to investigate the graphene-MoS_2 hybrid structures theoretically, we performed first-principles density functional theory (DFT) simulations.[8] As the lattice constant of isolated graphene is about 23% smaller than the one of isolated MoS_2, we constructed a supercell consisting of a 5x5 layer graphene (50 C atoms) coated with a 4x4 layer MoS_2 (16 Mo atoms and 32 S atoms) with a stacking as shown in Fig. 1b to account for this lattice mismatch. The remaining lattice mismatch of about 3-4% is reasonably small and compensated by a slight strain of graphene to the MoS_2 lattice constant.

The graphene-MoS_2 structure was then fully relaxed, which leads to an equilibrium graphene-MoS_2 distance of 3.35 Å in good agreement with Ref.[9] and indicates a weak interlayer bonding of van der Waals-type. Based on this setup, we simulated realistic edge and impurity effects on the electronic properties of graphene-MoS_2 hybrids.

We first address the role of impurity effects. To this end, we consider the fully MoS_2-covered graphene as in Fig. 1b without impurities and compare it to the case with impurities in the MoS_2. The band diagram of the pristine system is also shown in Fig. 1b. The green bands mark the graphene p_z contributions, and we see that the characteristic Dirac cone of graphene is preserved - with the Fermi level lying directly on the Dirac point. So, the interaction between graphene and clean MoS_2 is weak and does not induce an 'intrinsic' doping in the graphene[10] unlike e.g., SiC substrates.[11,12]

The situation can change when impurities are present in the MoS_2. Here, we consider Re atoms replacing Mo which naturally occur in MoS_2.[13,14] To simulate the effect of Re impurities, one Mo atom in the unit cell is replaced by a Re atom (Fig. 1c). We find that Re atoms substituting Mo atoms virtually do not alter the atomic structure of the system. In particular, the graphene-MoS_2 binding length and binding energy remain nearly the same. However, we see interesting electronic effects in the band diagram. Here, the Fermi level gets pinned at the impurity level in MoS_2, which leads to electron doping of graphene. The case depicted here, corresponds to a high impurity concentration of $7.6 \cdot 10^{13}$ cm^{-2} and shows a Fermi-level shift of 0.29 eV, which corresponds to an electron doping of $0.8 \cdot 10^{13}$ cm^{-2} . For an impurity concentration of $1.9 \cdot 10^{13}$ cm^{-2} (using a larger supercell) we find a shift of 0.27 eV. Thus, indicating that the doping saturates for impurity concentrations on the order of 10^{13} cm^{-2} which is a result of the linear density of states in graphene and the relative position of the impurity level in MoS_2. The Re d states are responsible for the electron transfer as can be seen from the red fat bands in Fig. 1c. These form broad donor levels and pin the Fermi level whereby the Dirac points become shifted toward the MoS_2 conduction bands. The hybridization between MoS_2 and graphene remains weak and keeps the graphene dispersion unaffected near the Dirac point. Also the binding energy remains unchanged compared to pristine MoS_2. Hence, the Re impurities within the MoS_2 provide the electrons for an n-type doping of graphene.

In order to verify the doping effect in graphene under MoS_2 experimentally, Raman spec-

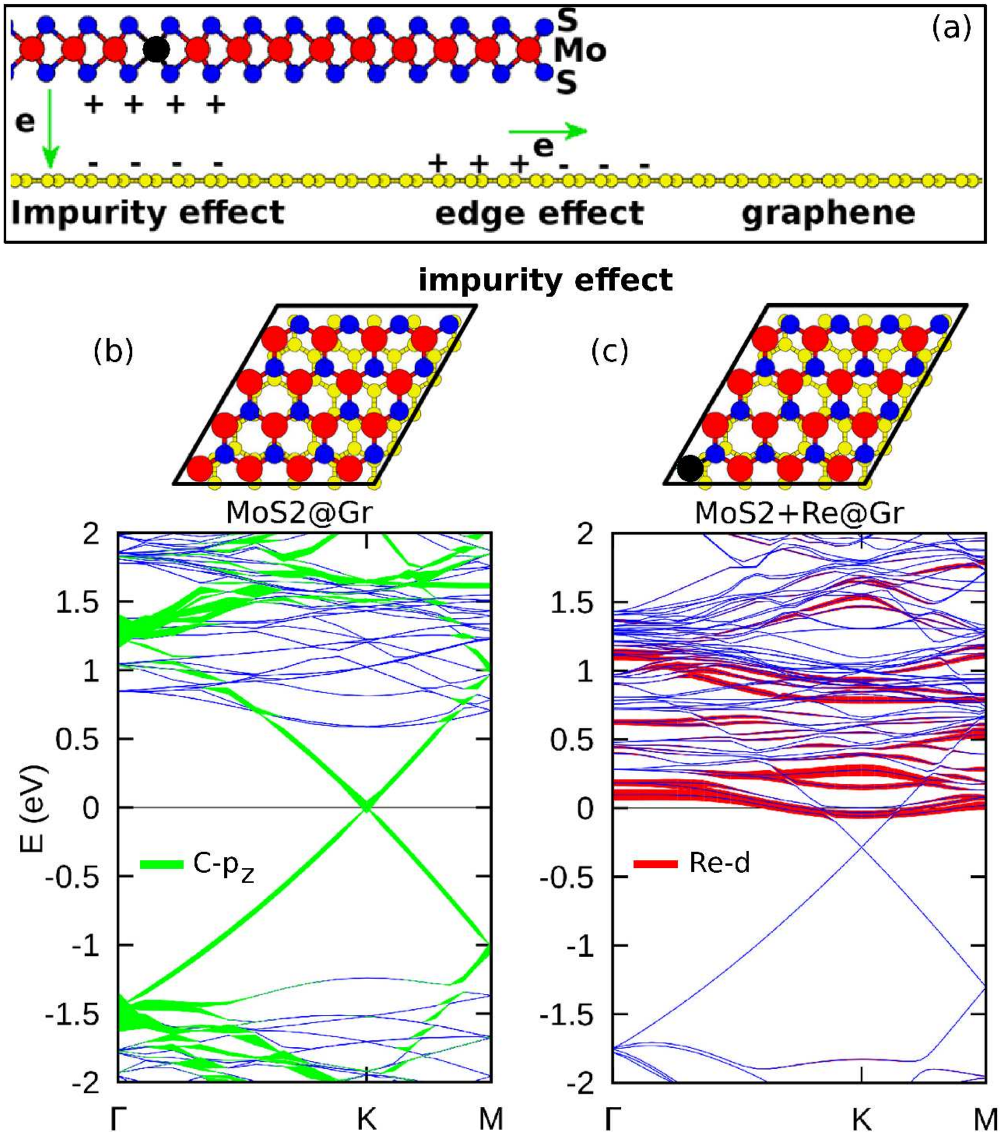

Figure 1: (a) Sketch of the graphene-MoS_2 system from side view with visualization of planar and impurity doping mechanisms. (b) (upper panel) Unit cell of graphene fully covered with MoS_2 from top view. Yellow atoms indicate the graphene carbon atoms, blue atoms sulfur and red atoms molybdenum. The stacking is chosen to be such that one C atom in the unit cell sits exactly below a Mo atom. In ref.[9] it is stated that another configuration, where C sits below an S atom, is equivalent in both the binding and electronic properties. (lower panel) Band structure of the system. The green fat bands visualize the graphene p_z bands. (c) The same system with Re impurities (black atom in the unit cell). The red fat bands visualize contributions of the Re d orbitals to the band structure. The Fermi level has been set to zero in both diagrams.

troscopy measurements were performed. Raman Spectroscopy has proven to be a facile and versatile technique to investigate graphene.[15] Crucially here, the Raman spectrum of graphene is susceptible to changes in the doping level.[16] The Raman spectrum of pristine and undoped graphene measured with a laser excitation energy of 2.5 eV consists of two important peaks,[17] the G and $2D$ peaks that are positioned at about 1580 cm^{-1} and 2700 cm^{-1}, respectively. Doping affects both peaks but has a more significant effect on the G peak:[16] for an increasing concentration of charge carriers, either holes or electrons, the position (Pos) of the G peak shifts to higher wavenumbers while its Full Width at Half Maximum (FWHM) decreases. Here we performed Raman mapping with a Witec spectrometer on a graphene strip partially covered with a $\mathrm{MoS_2}$ flake (Fig. 2a, for preparation details, see[18]). The spectral resolution achieved here is 3 cm^{-1}. The G and the $2D$ peaks were fitted with single Lorentzian peaks to extract the position, FWHM and integrated areas (A). The Raman spectrum of $\mathrm{MoS_2}$ has several features. Here, we used its out-of-plane $A_{1\mathrm{g}}$ mode to confirm the presence of $\mathrm{MoS_2}$.

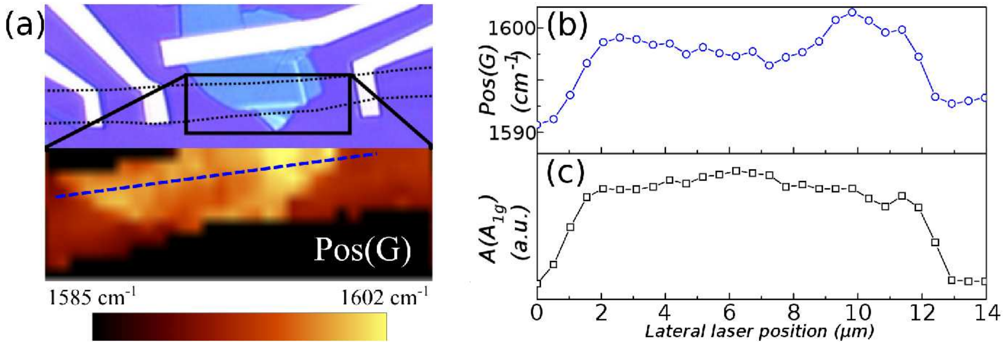

Figure 2: (a) Raman map (lower panel) of the sample region highlighted by a black box (upper panel). (b) G peak position as a function of the laser position along the path shown in (a, blue dashed line). (c) Integrated area $A(A_{1\mathrm{g}})$ of the $\mathrm{MoS_2}$ out-of-plane mode $A_{1\mathrm{g}}$ along the same path.

The FWHM(G) was seen to decrease from 15 cm^{-1} in the uncovered region to 9 cm^{-1} below the $\mathrm{MoS_2}$ flake. Simultaneously, we observed a blueshift of $Pos(G)$, confirming the doping effect of $\mathrm{MoS_2}$. Fig. 2a shows a spatially resolved map of $Pos(G)$. The shift of $Pos(G)$ over the whole area covered by $\mathrm{MoS_2}$ with respect to the uncovered graphene region can be clearly seen. Line scans (denoted by the blue dashed line) of $Pos(G)$ of graphene, and the integrated area $A(A_{1\mathrm{g}})$ of $\mathrm{MoS_2}$ are shown in plots 2b and 2c. The similar curve progressions of $Pos(G)$ and $A(A_{1\mathrm{g}})$

confirm the presence of MoS_2 along the scanned line. The largest shift of $Pos(G)$ is about 10 cm^{-1}, corresponding to a shift in the Fermi energy of about 0.3 eV.[16] This is well in line with our theoretically predicted Fermi level shift of 0.27–0.29 eV (the n-type of the doping is proven below). We further see that the G peak shift is rather constant in the whole MoS_2-covered region over a length of more than 10 μm, which indicates homogeneous doping. This is again in agreement with the scenario of Re impurities in MoS_2.

To recapitulate so far, we have shown that impurities in MoS_2 give rise to a charge transfer in vertical direction with a homogeneous distribution of the carriers in the plane. For a more complete picture of the interface physics, one also has to consider charge redistributions within the graphene plane due to MoS_2 edges. Therefore, we have simulated graphene where one half of the graphene-plane is covered with MoS_2. A supercell containing about 600 atoms was constructed[19] whereby three realistic MoS_2 edge configurations[20,21] were considered: the S-terminated $(\bar{1}010)$ edge and two Mo-terminated $(10\bar{1}0)$ edges with additionally adsorbed S dimers or S monomers. Fig. 3 sketches the case of an S-terminated $(\bar{1}010)$ edge.

The onsite-energy differences ΔE of p_z orbitals in graphene atoms near this edge with pristine MoS_2 are visualized in Fig. 3a. A potential gradient at the edge (dark green line) can be observed with a maximum height difference of almost 400 meV. Similar to the case of graphene with metal contacts, which generally show a work function difference at the interface between graphene and metal/graphene regions,[22] an electric field builds up which results in charge separation, i.e. a p-n junction. We emphasize here that the shape of the potential gradient varies with the edge structure. For instance, we find the potential step to be smaller at the Mo-terminated $(10\bar{1}0)$ edges. If impurities like Re are present in the MoS_2, the potential gradients created by work function differences at the edges are superimposed by bulk doping induced differences in the Fermi levels. This can be seen from the charge redistribution at this edge shown in Fig. 3b. For both, pristine and Re-contaminated MoS_2, a zone of lower occupation occurs near the potential step at 32 Å. In the pristine case (red dots) the uncovered graphene exhibits lower on-site energies and therefore gets locally n-doped while the MoS_2-covered part is p-doped with the exception of some single C atoms

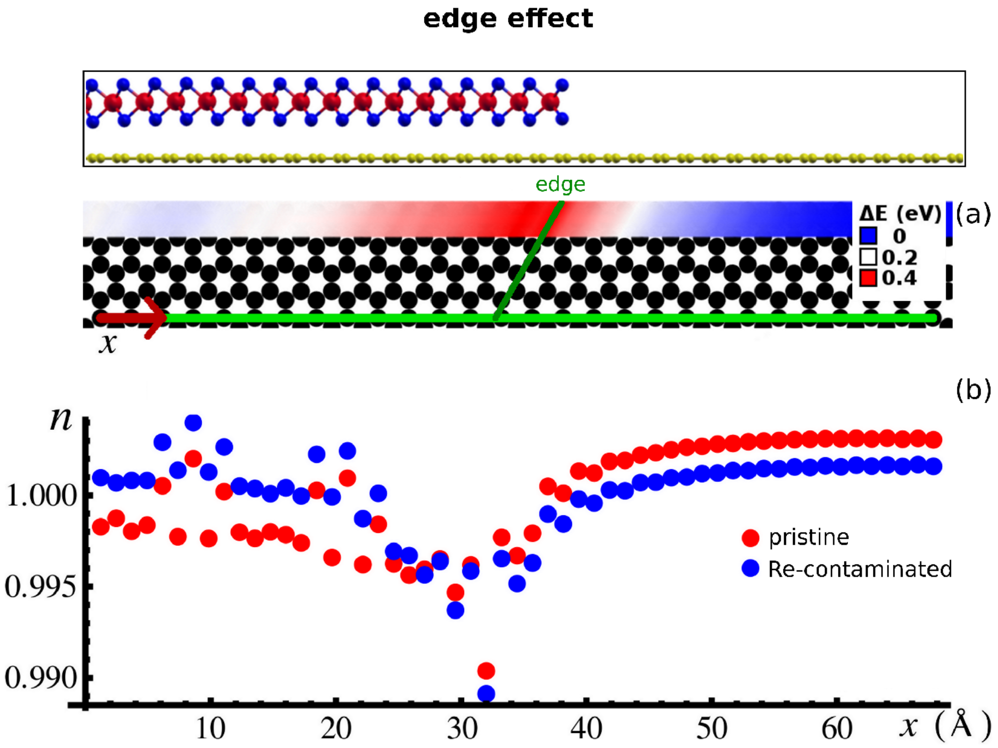

Figure 3: (a) Visualization of the on-site energies in graphene under a MoS_2 edge for the case of pristine MoS_2 (black dots denote graphene atoms, Mo and S atoms are not shown for clarity). ΔE is defined as the energy relative to the minimum p_z energy (far away from the edge in uncovered graphene). (b) Occupation of graphene p_z orbitals along the green line in (a) for pristine (red) and Re-contaminated (blue) MoS_2 ($n > 1$ means n-doping, the max. of $n = 1.004$ corresponds to $1.5 \cdot 10^{13} cm^{-2}$ carrier concentration).

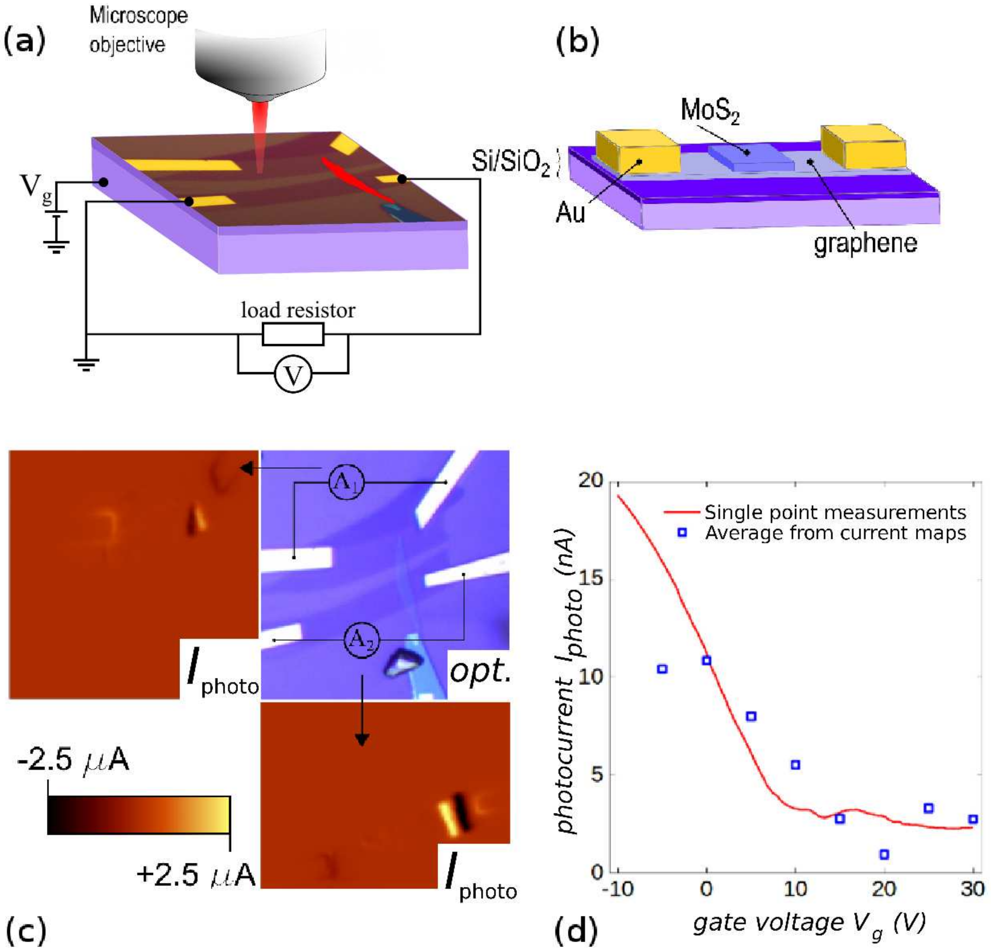

Figure 4: (a) Sketch of the experimental setup for photocurrent measurements. Graphene (brown stripes) is partially covered with MoS_2 flakes (red stripe) with gold contacts (yellow) and irradiated by a laser beam). (b) Sketch of a lateral cut through the sample for clarity. (c) Photocurrent maps with the terminals connected to the top (left top panel) or bottom (right bottom panel) electrodes. The dark blue stripes indicate graphene, the narrow light blue stripe in perpendicular direction denotes the MoS_2 stripe. (d) Dependence of the photocurrent I_{photo} from the gate voltage V_{g} (see text) from static point measurements (solid red line) and current maps averages (blue squares).

that sit below the middle of a MoS_2 hexagon (cf. Fig. 1b). This charge reordering is restricted to regions close to the edge, and under perfect conditions graphene is undoped on both sides at large distance. However, in a realistic system, Re impurities in the MoS_2 are present. Then the situation at the $(\bar{1}010)$ edge is different: for a Re contamination as discussed above, the n-type bulk doping effect of MoS_2 on graphene and the edge-induced local p-doping compete. As a result, also the MoS_2-covered side becomes electron-doped in the edge region (Fig. 3b, blue dots).

To gain experimental insight into potential gradients at edges, we performed photocurrent measurements (Fig. 4a and b). Therefore, the sample was placed on a piezoelectric stage below a 1.96 eV (633 nm) laser. The current flowing in a circuit comprised the photoactive graphene - MoS_2 heterostructure and was measured as a function of the piezoelectric stage position. The laser power was set at 80 μW and the laser spot radius was 0.5 μm. As has been previously reported,[23] there is a photovoltaic current generated at the interface between metal contacts and graphene due to the p - n junctions. Similarly, we measure a clear photocurrent signal when the laser spot is in the region where the MoS_2 has been placed (red region, Fig. 4a), while virtually no measurable current is generated in the uncovered graphene (purple region) and only a small current near the metal contacts (yellow regions). The measurements are shown in Fig. 4c and d. In 4c, photocurrent maps are recorded when the terminals are connected to either the top or bottom two electrodes respectively (top left and bottom right panel). The scanning photocurrent data was measured by recording the voltage drop across a load resistor of known resistance placed in series with the device. The response was determined for each step in the x-y position of the laser by measuring the voltage across this resistor. In this fashion, a spatial map of the local photocurrent distribution could be produced. In the top right panel an optical image of the device is shown. The photocurrent generated at the graphene - Au interface can be seen while a much stronger signal is obtained on the graphene - MoS_2 heterostructure. Also in some regions of uncovered graphene a small photocurrent is present due to small variations in local doping, but the effect is too minor to be visible on this scale.

The symmetry of the photocurrent maps shows that the current is generated at the interface between the uncovered and the MoS_2-covered region. Since the uncovered graphene is undoped while it is n-doped when covered with $\mathrm{MoS_2}$, a potential barrier builds up as discussed above. The resulting electric field prevents a recombination of laser-induced electron-hole pairs and finally results in a current. Hence, it is the interplay of impurity doping and potential gradients that permits to use the graphene-$\mathrm{MoS_2}$ heterostructure as a photodetector. Importantly, the current is not generated near the metal contacts like in most graphene-based photodetectors.[23–26] The photocurrent generated in a certain region of the sample is proportional to the local potential gradients. Therefore, the photocurrent map depicts local potential gradients and reveals the spatial dependence of the Fermi level. This technique is thus a powerful tool to investigate the doping levels in graphene heterostructures with spatial resolution.

The photocurrent signal I_{photo} of the active region responds to a gate voltage V_{g} (Fig. 4d), and approaches a small constant value at ~ 30 V which corresponds to an electron concentration of $2 \cdot 10^{12}\mathrm{cm}^{-2}$. The response of I_{photo} to V_{g} was measured in two ways: i. the laser was statically positioned on the heterostructure (solid red line) while sweeping gate voltage. ii. photocurrent maps were taken at a series of different gate voltage values and the mean current from the active region calculated (blue squares). For these measurements a potential was applied between the silicon backgate and graphene, while the graphene was kept grounded.[27] For negative gate voltages the photocurrent signal increased, which corresponds to an increased potential step at the edges. For positive gate voltages, the photocurrent signal decreased until the heterostructure region was barely distinguishable. Since a positive sign of V_{g} corresponds to an electron doping, this confirms the n-type doping of graphene under $\mathrm{MoS_2}$. This is also in agreement with ref.,[28] where an n-type doping of graphene on $\mathrm{MoS_2}$ is reported.

Apparently, the potential barrier changes upon applying a gate voltage V_{g}. The local Fermi level in $\mathrm{MoS_2}$-covered and uncovered graphene responds differently to V_{g}. This is because the $\mathrm{MoS_2}$ on graphene can partially screen the gate induced electric fields due to quantum capacitance related charge redistributions from graphene to $\mathrm{MoS_2}$ (Fig. 5): in uncovered graphene, all charge density ρ induced by V_{g} has to be taken up by the graphene bands. Thus, the Fermi level in graphene increases correspondingly to ρ. On the contrary, in $\mathrm{MoS_2}$-covered graphene in addition to states

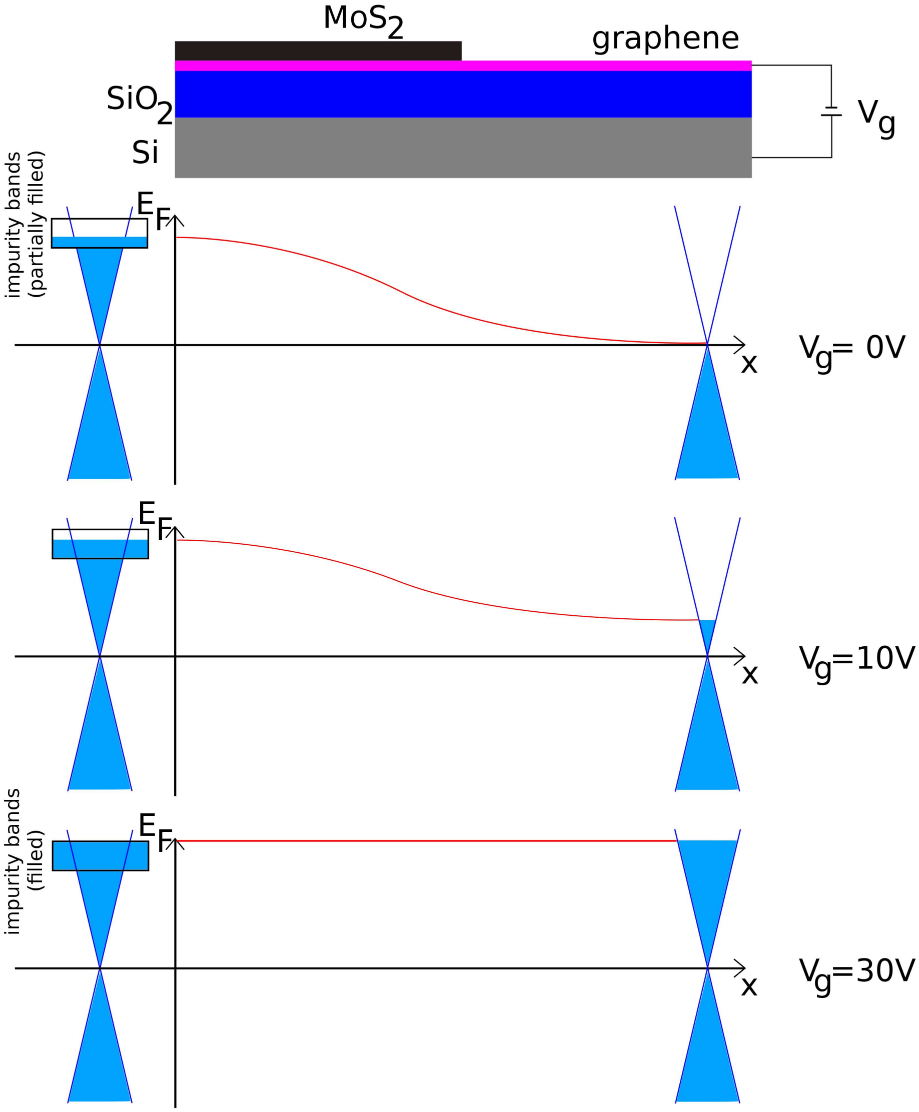

Figure 5: (a) Illustration of the Fermi level evolution along the MoS_2 edge for different gate voltages V_g. In the MoS_2-covered region (left), the Fermi level becomes pinned due to impurity bands while it increases in the uncovered region (right) with V_g.

derived from graphene, MoS_2 states or impurity states from MoS_2 can be available at the Fermi level. These latter MoS_2 and impurity-derived states take up large parts of the charge (due to the low density of states in graphene) and thus, the gate voltage-induced changes of the Fermi level are much smaller in the uncovered than in the covered region. In other words, impurity levels in MoS_2 induce a Fermi level pinning as discussed in Fig. 1c. This mechanism is responsible for high photocurrents at negative gate voltages: the uncovered graphene becomes hole-doped while the MoS_2-covered region remains with the Fermi level pinned to the Re donor states. Thus, the potential step at the MoS_2 edges increases with negative gate voltages which amplifies the photocurrent. For positive gate voltages, the Fermi level in uncovered graphene increases and the potential step is reduced. At very large gate voltages, we speculate that the Re donor bands become filled and there is essentially no charge transfer from the donor bands to graphene. Therefore, the potential step and the photocurrent generated at the MoS_2 edge become very small.

In conclusion, we presented an investigation of graphene-MoS_2 hybrid structures. Our DFT calculations reveal two different doping mechanisms: First, we showed that MoS_2 edges induce charge redistributions within the graphene plane. Second, Re impurities in the MoS_2 lead to charge transfer from MoS_2 to the graphene. Raman and photovoltaic experiments support these findings. The interplay of impurity as well as edge effects allows to build graphene-MoS_2 photodetector devices where the photocurrent is not generated at the metal contacts.

Funding by the Deutsche Forschungsgemeinschaft via SPP 1459 is acknowledged.

Notes and References

(1) Novoselov, K. S.; Jiang, D.; Schedin, F.; Booth, T. J.; Khotkevich, V. V.; Morozov, S. V.; Geim, A. K. *PNAS* **2005**, *102*, 10451–10453.

(2) Ponomarenko, L. A.; Geim, A. K.; Zhukov, A. A.; Jalil, R.; Morozov, S. V.; Grigorieva, I. V.; Novoselov, K. S.; Hill, E. H.; Cheianov, V. V.; Falko, V. I.; Watanabe, K.; Taniguchi, T.; Gorbachev, R. V. *Nature Phys.* **2011**, *7*, 958–961.

(3) Britnell, L.; Gorbachev, R. V.; Jalil, R.; Belle, B. D.; Schedin, F.; Mishchenko, A.; Georgiou, T.; Katsnelson, M. I.; Eaves, L.; Morozov, S. V.; Peres, N. M. R.; Leist, J.; Geim, A. K.; Novoselov, K. S.; Ponomarenko, L. A. *Science* **2012**, *335*, 947–950.

(4) Ponomarenko, L. A.; Yang, R.; Mohiuddin, T. M.; Katsnelson, M. I.; Novoselov, K. S.; Morozov, S. V.; Zhukov, A. A.; Schedin, F.; Hill, E. W.; Geim, A. K. *Phys. Rev. Lett.* **2009**, *102*, 206603.

(5) Dean, C. R.; Young, A. F.; Meric, I.; Lee, C.; Wang, L.; Sorgenfrei, S.; Watanabe, K.; Taniguchi, T.; Kim, P.; Shepard, K. L.; Hone, J. *Nature Nanotech.* **2010**, *5*, 722–726.

(6) Novoselov, K. S. *Rev. Mod. Phys.* **2011**, *83*, 837–849.

(7) Wang, Q. H.; Kalantar-Zadeh, K.; Kis, A.; Coleman, J. N.; Strano, M. S. *Nature Nanotech.* **2012**, *7*, 699–712.

(8) The DFT calculations were performed using the Vienna ab initio simulations package (VASP)[29] with projector augmented (PAW) plane waves.[30,31] The local density approximation (LDA) was employed to the exchange-correlation potential, which is better suited to describe van der Waals forces in weakly bound layered systems than generalized gradient (GGA) functionals.[32–34] A k-mesh of 12x12x1 points and a plane-wave cut-off of 500 eV was employed.

(9) Ma, Y.; Dai, Y.; Guo, M.; Niu, C.; Huang, B. *Nanoscale* **2011**, *3*, 3883–3887.

(10) The only effect of MoS_2 on the low-energy states we see in a close-up is a small band gap of less than 1 meV respectively 2 meV with Re impurities. This is supposed to be analogous to the case of graphene on boron nitride, where small finite band gaps can occur due to local mass terms in the moiré cell.[33] However, this gap is too small to limit electron mobility significantly.

(11) Ristein, J.; Mammadov, S.; Seyller, T. *Phys. Rev. Lett.* **2012**, *108*, 246104.

(12) Kim, S.; Ihm, J.; Choi, H.; Son, Y.-W. *Phys. Rev. Lett.* **2008**, *100*, 176802.

(13) Stellman, J. *Encyclopaedia of occupational health and safety*; Intl Labour Organisation, 1998.

(14) Greenwood, N.; Earnshaw, A. *Chemistry of the Elements (2nd ed.)*; Butterworth-Heinemann, 1997.

(15) Casiraghi, C. *Spectroscopic properties of inorganic and organometallic compounds*; Royal Society of Chemistry, 2012; Vol. 43; p 29.

(16) Das, A.; Pisana, S.; Chakraborty, B.; Piscanec, S.; Saha, S. K.; Waghmare, U. V.; Novoselov, K. S.; Krishnamurthy, H. R.; Geim, A. K.; Ferrari, A. C.; Sood, A. K. *Nature Nanotech.* **2008**, *3*, 210–215.

(17) Ferrari, A. C.; Meyer, J. C.; Scardaci, V.; Casiraghi, C.; Lazzeri, M.; Mauri, F.; Piscanec, S.; Jiang, D.; Novoselov, K. S.; Roth, S.; Geim, A. K. *Phys. Rev. Lett.* **2006**, *97*, 187401.

(18) The measurements were performed on samples comprised of a graphene - MoS_2 heterostructure with Au electrodes contacting the graphene. The samples were prepared by first mechanically cleaving a graphene flake onto a Si/SiO_2 (300 nm oxide layer) substrate.[35] A separately prepared MoS_2 flake was then transferred to the surface of the graphene flake. For this, a dry transfer technique[5] was used whereby the MoS_2 was prepared on a polymer substrate, inverted and placed in the chosen position to ensure a clean interface between the two materials. Au contacts were then fabricated by standard photolithographic processing.

(19) For this purpose, the unit cell in Fig. 3a was repeated 8 times in one direction, whereby only half of the supercell was covered by MoS_2. Here, a 3x1x1 k-mesh was selected together with a plane-wave cut-off of 400 eV. Rhenium impurities were included in the same concentration as discussed in Fig. 1 with a minimum distance of Re impurities to the MoS_2 edge of about 10 Å.

(20) Bollinger, M. V.; Lauritsen, J. V.; Jacobsen, K. W.; Nørskov, J. K.; Helveg, S.; Besenbacher, F. *Phys. Rev. Lett.* **2001**, *87*, 196803.

(21) Bollinger, M. V.; Jacobsen, K. W.; Nørskov, J. K. *Phys. Rev. B* **2003**, *67*, 085410.

(22) Khomyakov, P. A.; Starikov, A. A.; Brocks, G.; Kelly, P. J. *Phys. Rev. B* **2010**, *82*, 115437.

(23) Park, J.; Ahn, Y. H.; Ruiz-Vargas, C. *Nano Lett.* **2009**, *9*, 1742–1746.

(24) Xia, F.; Mueller, T.; Golizadeh-Mojarad, R.; Freitag, M.; Lin, Y.; Tsang, J.; Perebeinos, V.; Avouris, P. *Nano Lett.* **2009**, *9*, 1039–1044.

(25) Echtermeyer, T. J.; Britnell, L.; Jasnos, P. K.; Lombardo, A.; Gorbachev, R. V.; Grigorenko, A. N.; Geim, A. K.; Ferrari, A. C.; Novoselov, K. S. *Nat. Commun.* **2011**, *2*, 458–462.

(26) Lee, E. J. H.; Balasubramanian, K.; Weitz, R. T.; Burghard, M.; Kern, K. *Nature Nanotech.* **2008**, *3*, 486–490.

(27) For these measurements, a sample with several layers of MoS_2 without additional graphene layers on top was used, which explains the small photocurrent compared to Fig. 4d.

(28) Zhang, W.; Chuu, C.-P.; Huang, J.-K.; Chen, C.-H.; Tsai, M.-L.; Chang, Y.-H.; Liang, C.-T.; He, J.-H.; Chou, M.-Y.; Li, L.-J. *arXiv preprint arXiv:1302.1230* **2013**,

(29) Kresse, G.; Hafner, J. *J. Phys.: Condens. Matter* **1994**, *6*, 8245.

(30) Blöchl, P. E. *Phys. Rev. B* **1994**, *50*, 17953.

(31) Kresse, G.; Joubert, D. *Phys. Rev. B* **1999**, *59*, 1758.

(32) Tran, F.; Laskowski, R.; Blaha, P.; Schwarz, K. *Phys. Rev. B* **2007**, *75*, 115131.

(33) Sachs, B.; Wehling, T. O.; Katsnelson, M. I.; Lichtenstein, A. I. *Phys. Rev. B* **2011**, *84*, 195414.

(34) Hasegawa, M.; Nishidate, K. *Phys. Rev. B* **2004**, *70*, 205431.

(35) Novoselov, K. S.; Geim, A. K.; Morozov, S. V.; Jiang, D.; Zhang, Y.; Dubonos, S. V.; Grigorieva, I. V.; Firsov, A. A. *Science* **2004**, *306*, 666–669.